SUPPLEMENTARY MATERIAL

Bioactive xanthoquinodins and epipolythiodioxopiperazines from *Chaetomium globosum* 7s-1, an endophytic fungus isolated from *Rhapis cochinchinensis* (Lour.) Mart.

Cholpisut Tantapakul[a] , Trinop Promgool[a] , Kwanjai Kanokmedhakul[a] , Kasem Soytong[b] , Jiaojiao Song[b], Sarinya Hadsadee[c], Siriporn Jungsuttiwong[c] and Somdej Kanokmedhakul[a,*]

[a]*Natural Products Research Unit, Department of Chemistry and Center of Excellence for Innovation in Chemistry, Faculty of Science, Khon Kaen University, Muang, Khon Kaen 40002, Thailand;* [b]*Department of Plant Production Technology, Faculty of Agricultural Technology, King Mongkut's Institute of Technology Ladkrabang, Bangkok 10520, Thailand;* [c]*Center for Organic Electronic and Alternative Energy, Department of Chemistry and Center of Excellence for Innovation in Chemistry, Faculty of Science, Ubon Ratchathani University, Ubon Ratchathani 34190, Thailand*

Abstract:

A new xanthoquinodin B9 (**1**), together with two known xanthoquinodins, xanthoquinodin A1 (**2**) and xanthoquinodin A3 (**3**), three epipolythiodioxopiperazines, chetomin (**4**), chaetocochin C (**5**) and dethio-tetra(methylthio)chetomin (**6**), and four other compounds, chrysophanol (**7**), emodin (**8**), alatinone (**9**), and ergosterol (**10**) were isolated from the endophytic fungus *Chaetomium globosum* 7s-1, isolated from *Rhapis cochinchinensis* (Lour.) Mart. All isolated structures were established based on their spectroscopic data analyses. Compounds **1**−**6** showed antibacterial activity against Gram positive bacteria with MICs ranging from 0.02 pM to 10.81 μM. Compounds **1**−**6** also exhibited cytotoxicity against KB, MCF-7 and NCI-H187 cancer cell lines (IC_{50} 0.04−18.40 μM). However, they were cytotoxic towards a normal cell line (*Vero* cell) with IC_{50} values ranging from 0.04−3.86 μM.

Keywords: *Chaetomium globosum*; xanthoquinodin; epipolythiodioxopiperazine; antibacterial

List of Supplementary Materials **Page**

General experimental procedures

Melting points were determined on a SANYO MPU350BM3.5 melting point apparatus (SANYO Gallenkamp PLC, Leicestershire, UK) and were uncorrected. Optical rotations were determined on a JASCO DIP-1000 digital polarimeter (JASCO, Inc., Maryland, USA). IR spectra were recorded using a Bruker Tensor 27 FT-IR spectrometer (Agilent Technologies, USA). CD and UV spectra were measured using a JASCO J-810 apparatus. NMR spectra were obtained from a Varian Mercury Plus 400 (Varian, Inc., USA) and a Bruker AVANCE III 500 MHz (Bruker, Germany) spectrometers. Chemical shifts were recorded on a δ (ppm) scale using $CDCl_3$, CD_3OD, and DMSO-d_6 as solvents, and using residual of these solvents as an internal standard. HRESITOFMS spectra were acquired using a Micromass Q-TOF-2 spectrometer (Bruker, Germany). Column chromatography was carried out over Merck silica gel 60 (230−400 mesh) (Merck, Darmstadt, Germany). TLC was performed with precoated Merck silica gel 60 PF_{254} aluminium sheets (Merck, Darmstadt, Germany); the spots were visualized under UV light (254 and 366 nm) and further by spraying with anisaldehyde and then heating until charred.

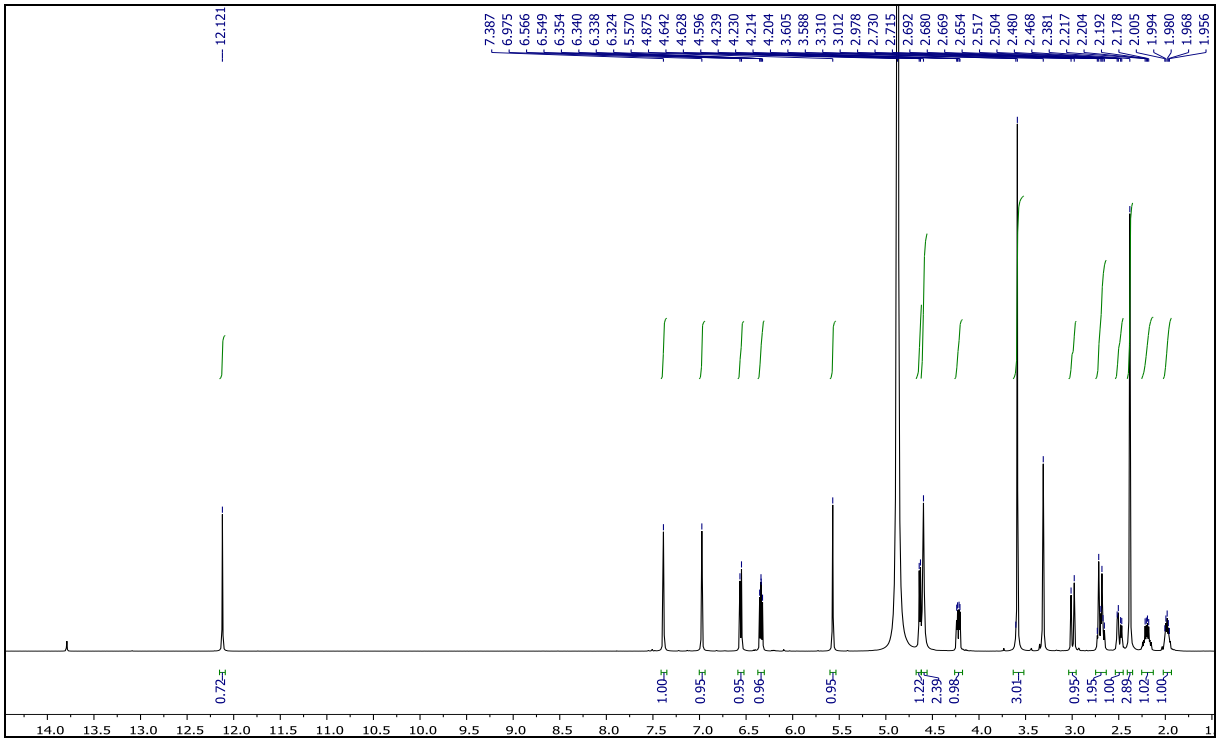

Figure S1. ^{1}H NMR spectrum of compound **1** (500 MHz, CD_3OD).

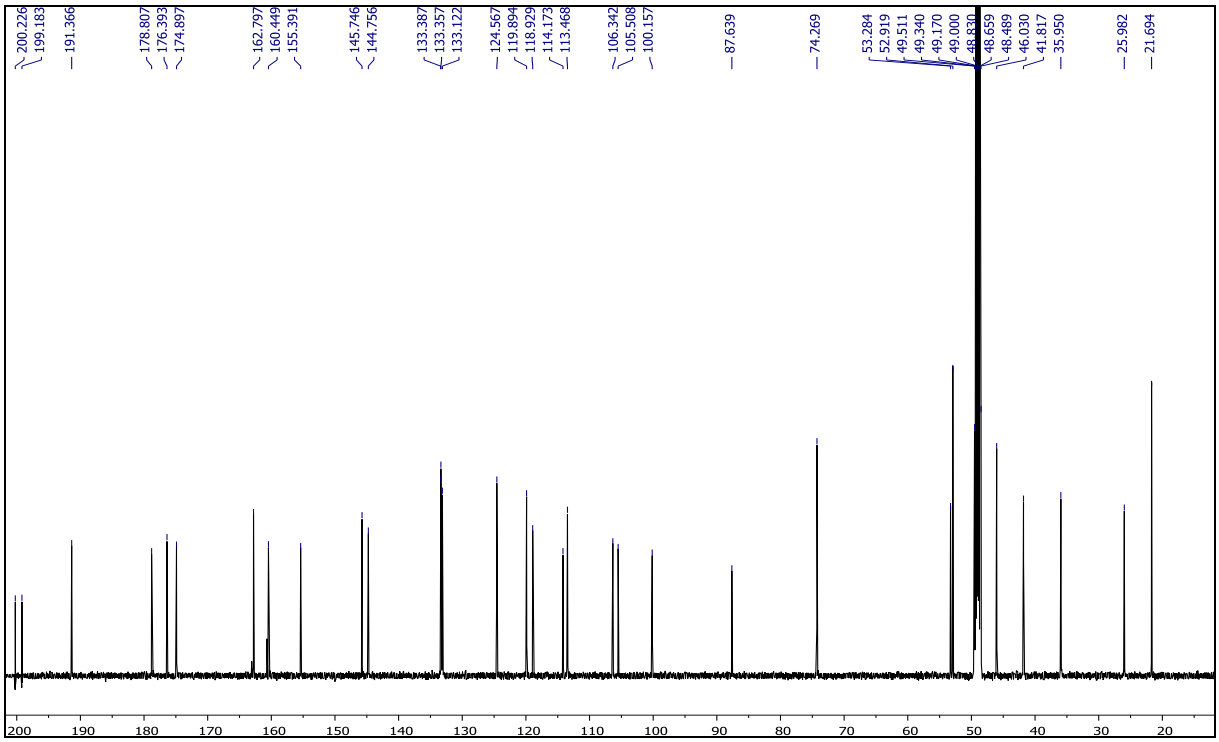

Figure S2. ^{13}C NMR spectrum of compound **1** (125 MHz, CD_3OD).

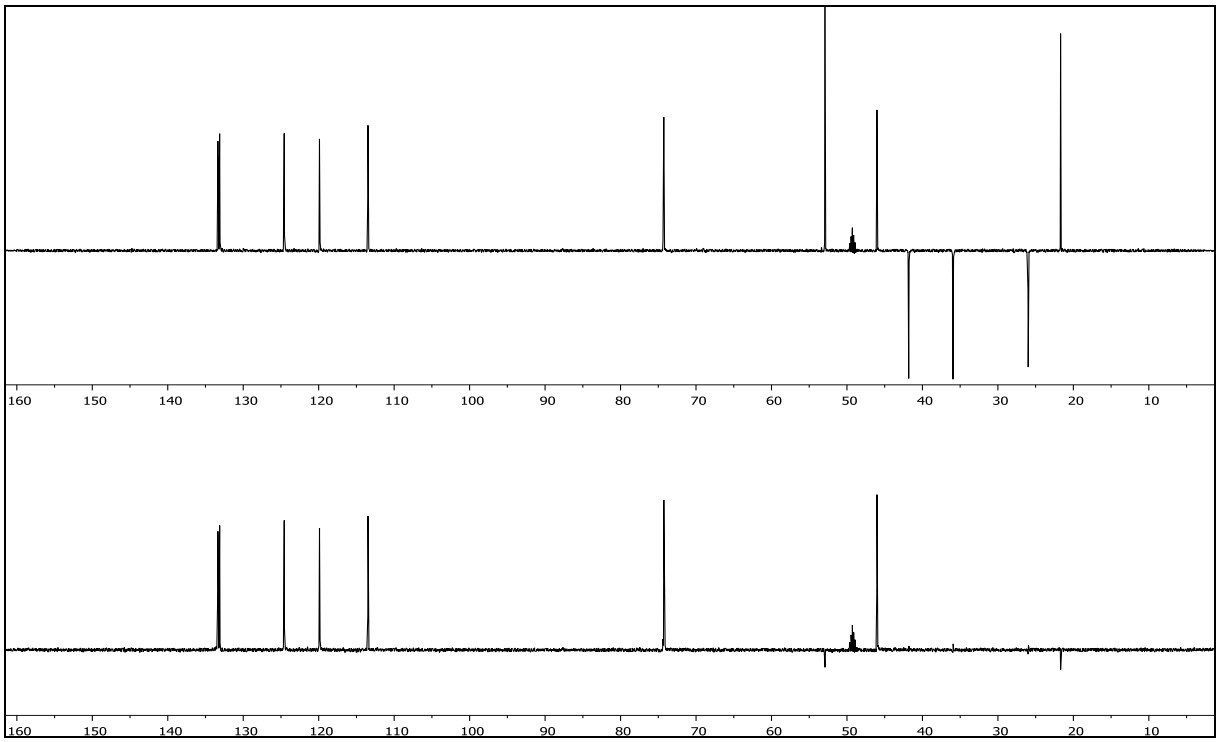

Figure S3. DEPT spectra of compound **1** (125 MHz, CD_3OD).

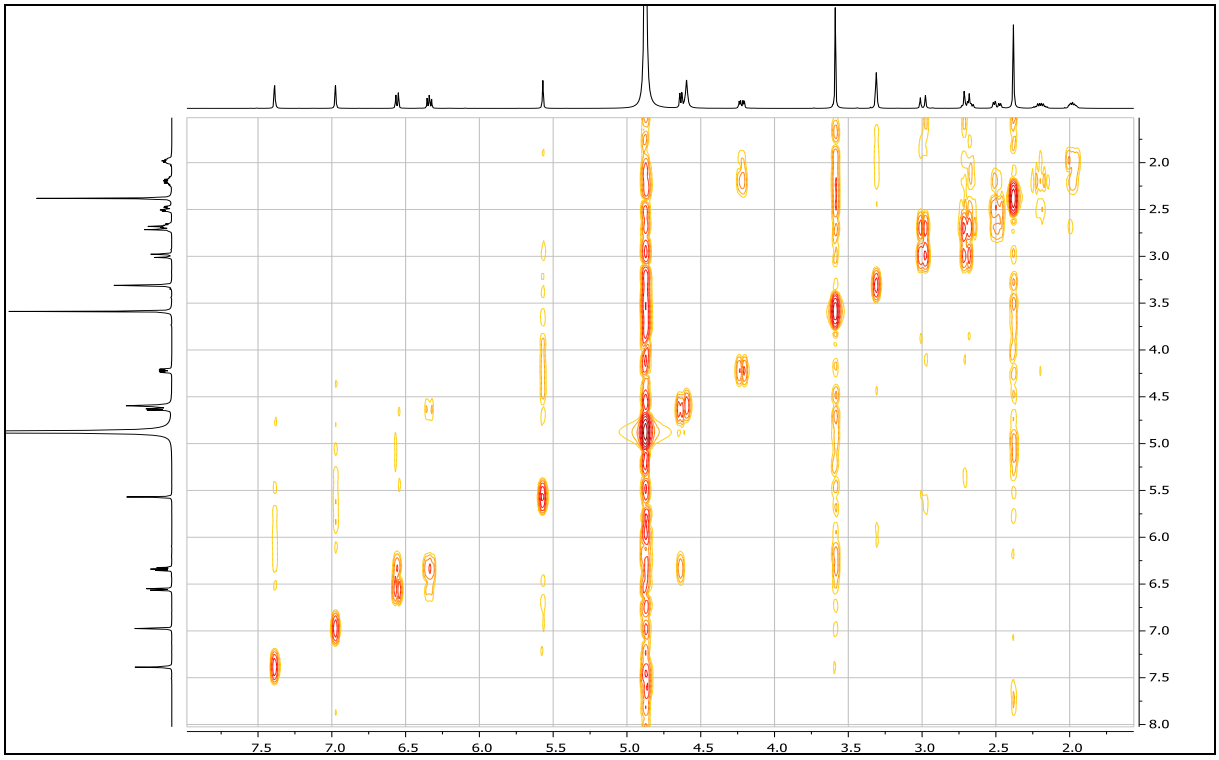

Figure S4. COSY spectrum of compound **1** in CD_3OD.

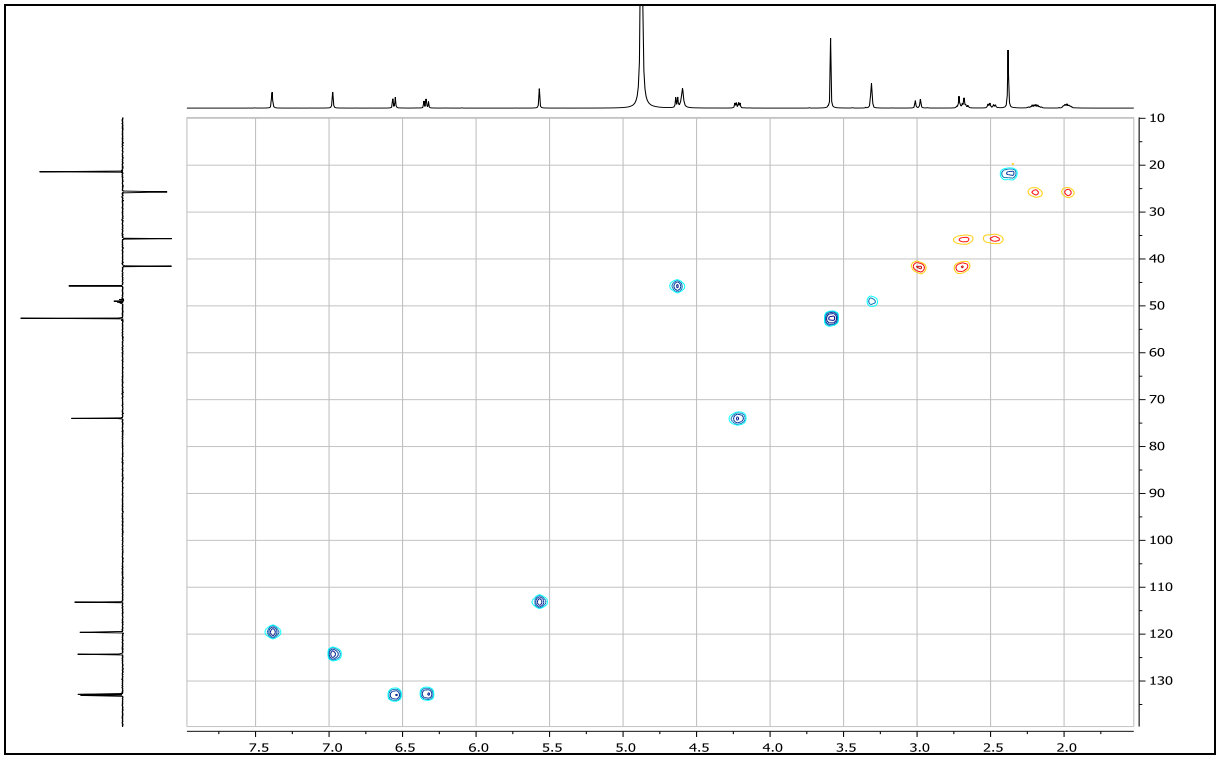

Figure S5. HSQC spectrum of compound **1** in CD_3OD**.**

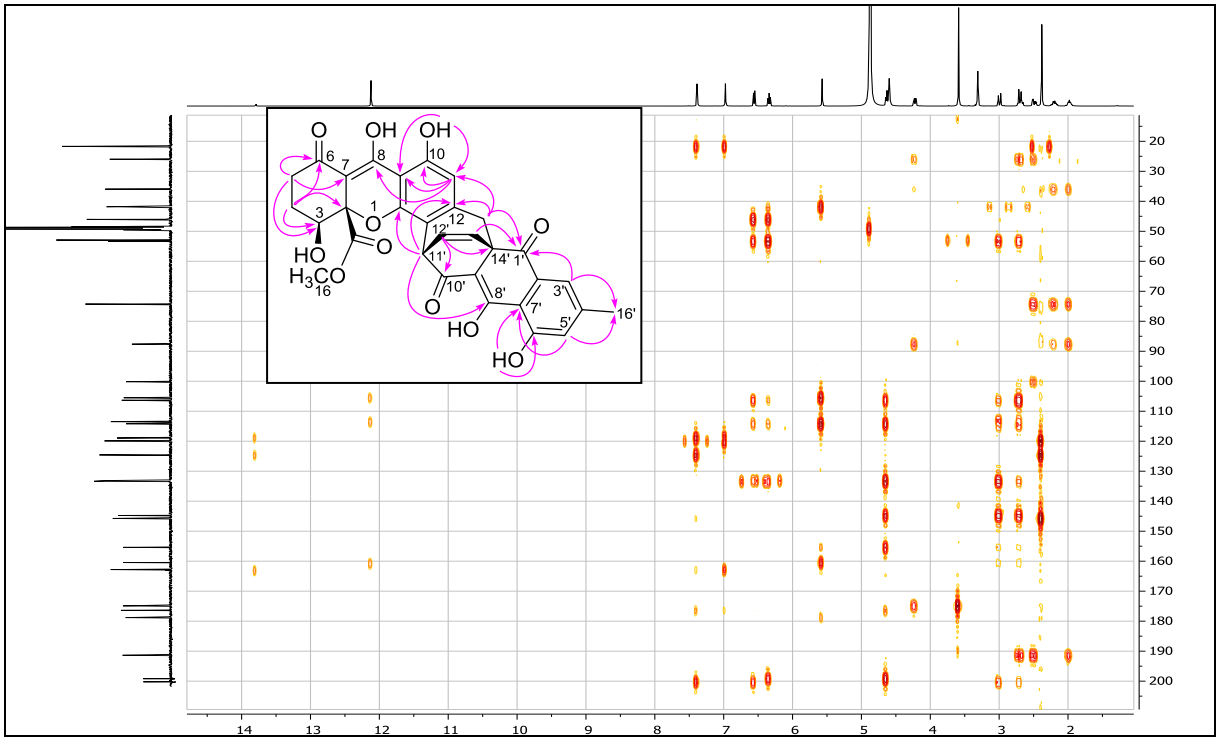

Figure S6. HMBC spectrum of compound **1** in CD_3OD.

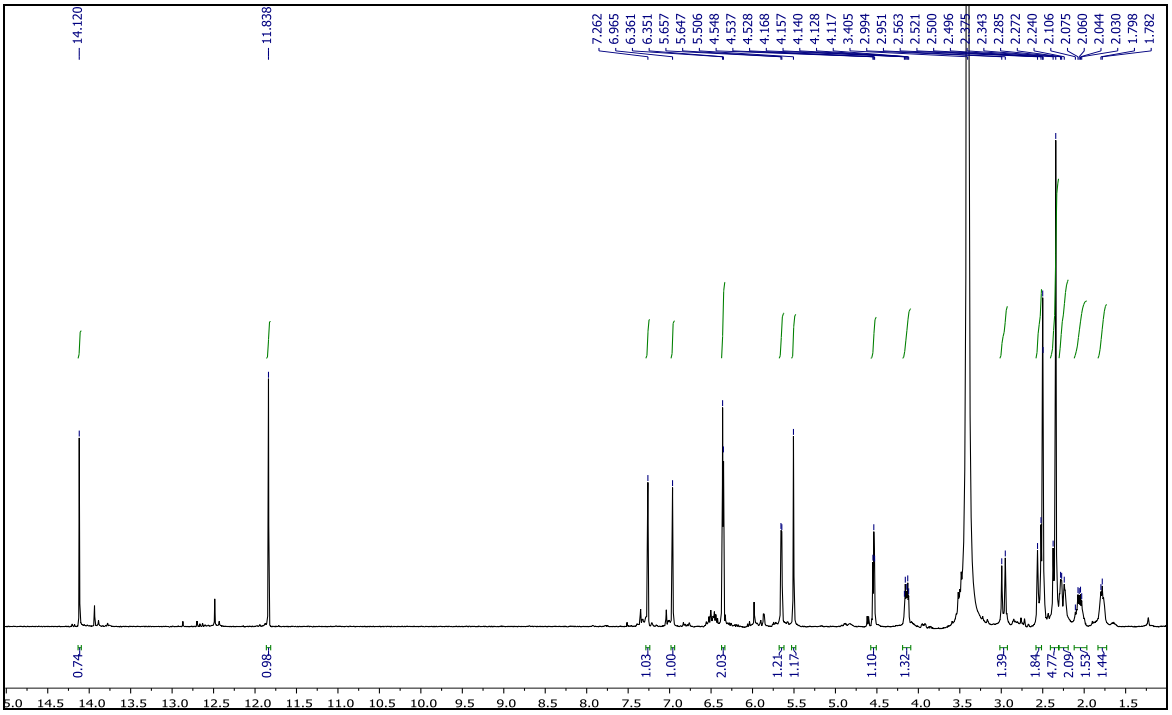

Figure S7. ^{1}H NMR spectrum of compound **1** (400 MHz, DMSO-d_6).

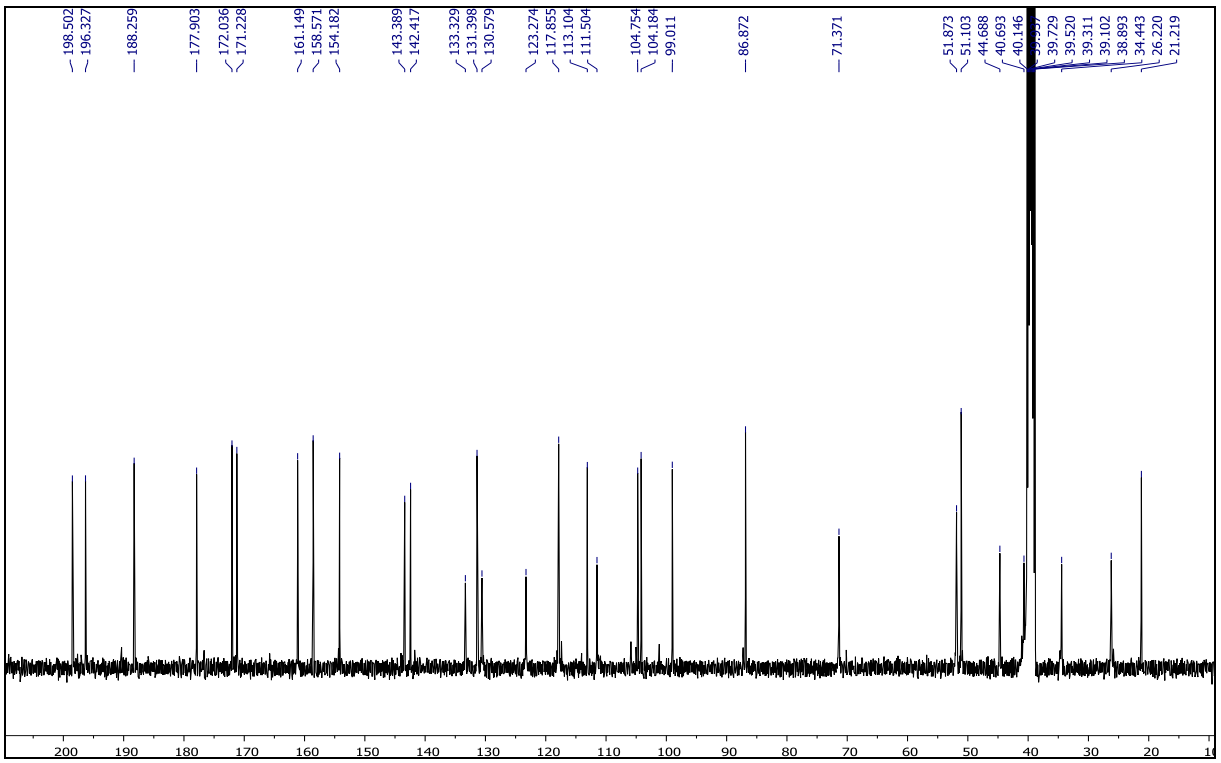

Figure S8. ^{13}C NMR spectrum of compound **1** (100 MHz, DMSO-d_6).

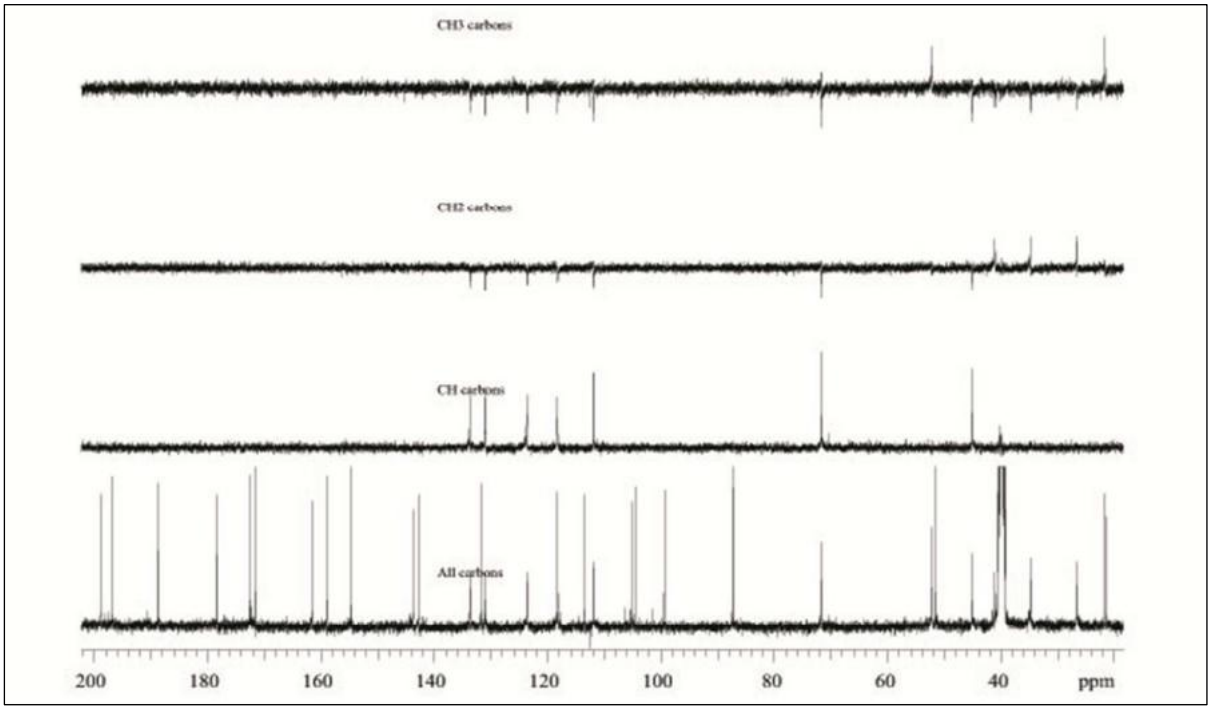

Figure S9. DEPT spectra of compound **1** (100 MHz, DMSO-d_6).

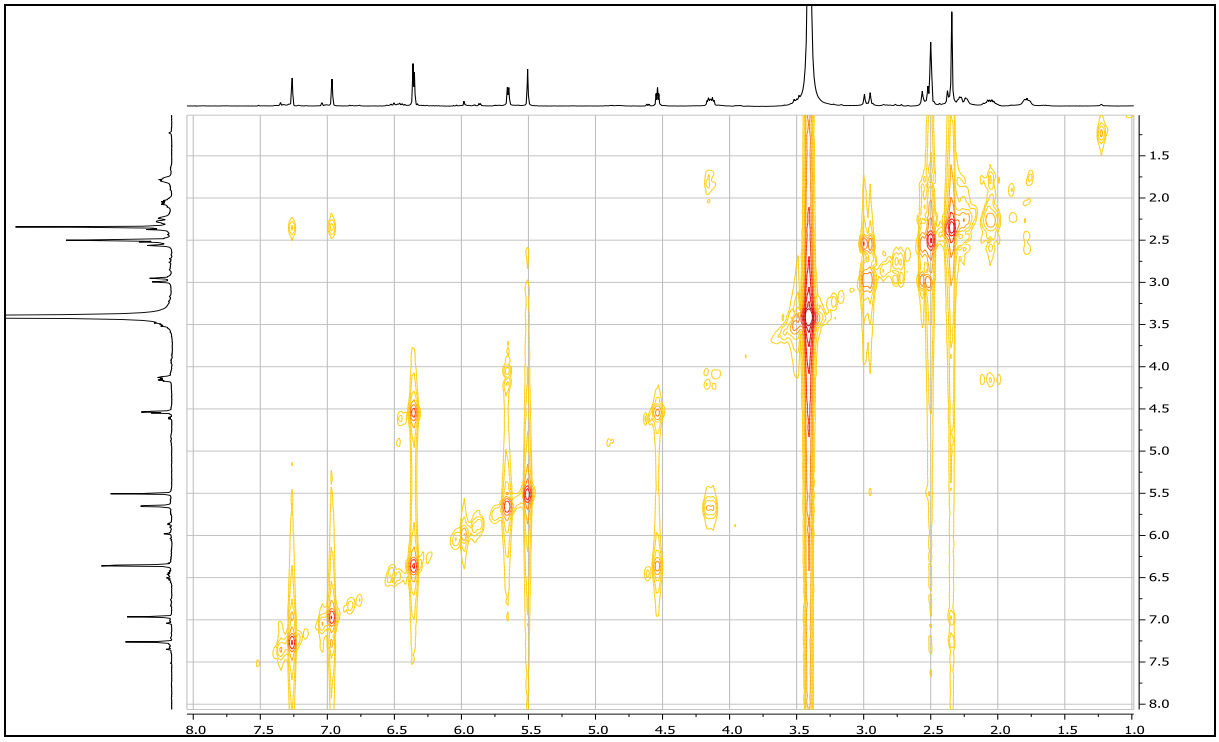

Figure S10. COSY spectrum of compound **1** in DMSO-d_6.

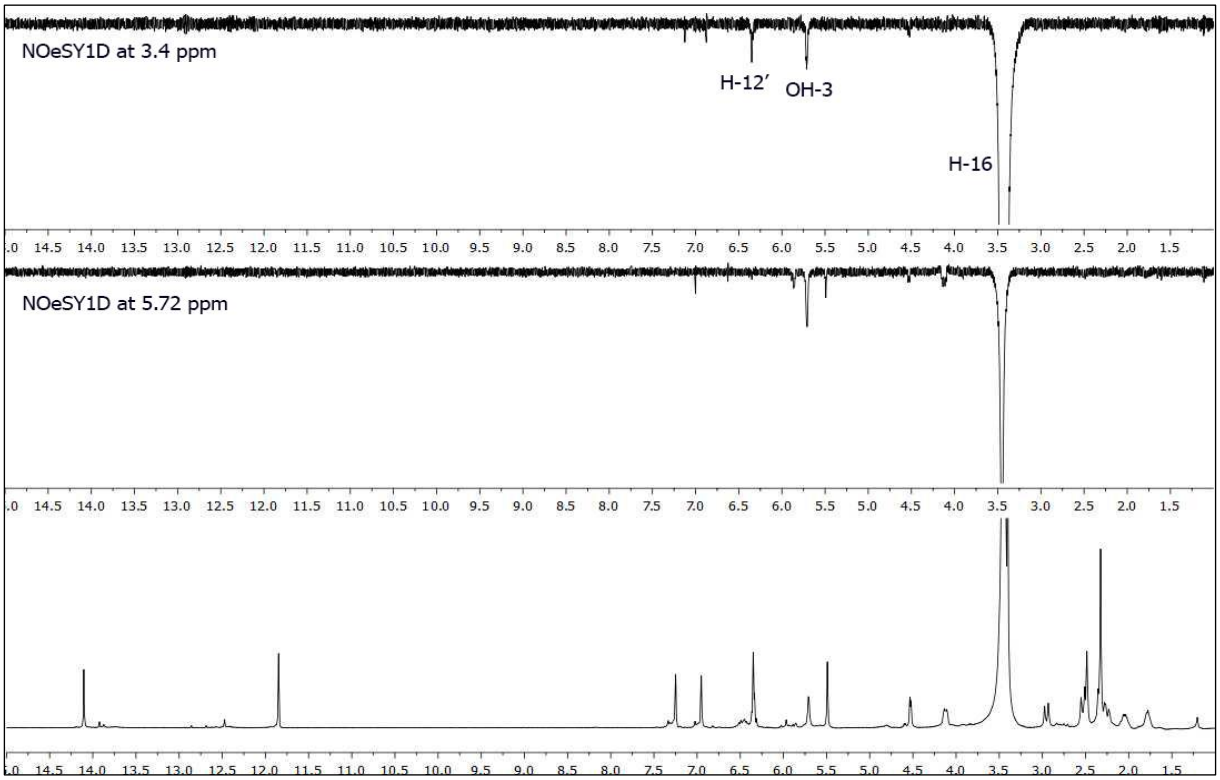

Figure S11. NOE spectrum of compound **1** in DMSO-d_6

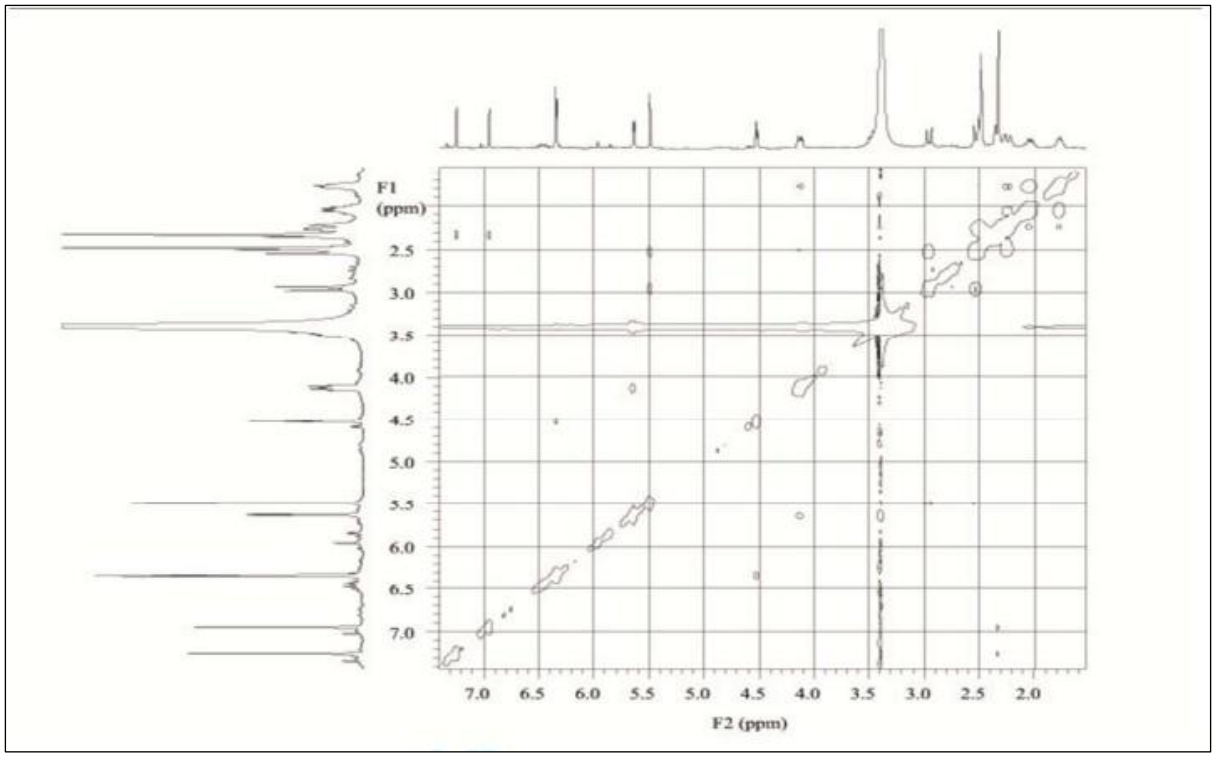

Figure S12. NOESY spectrum of compound **1** in DMSO-d_6.

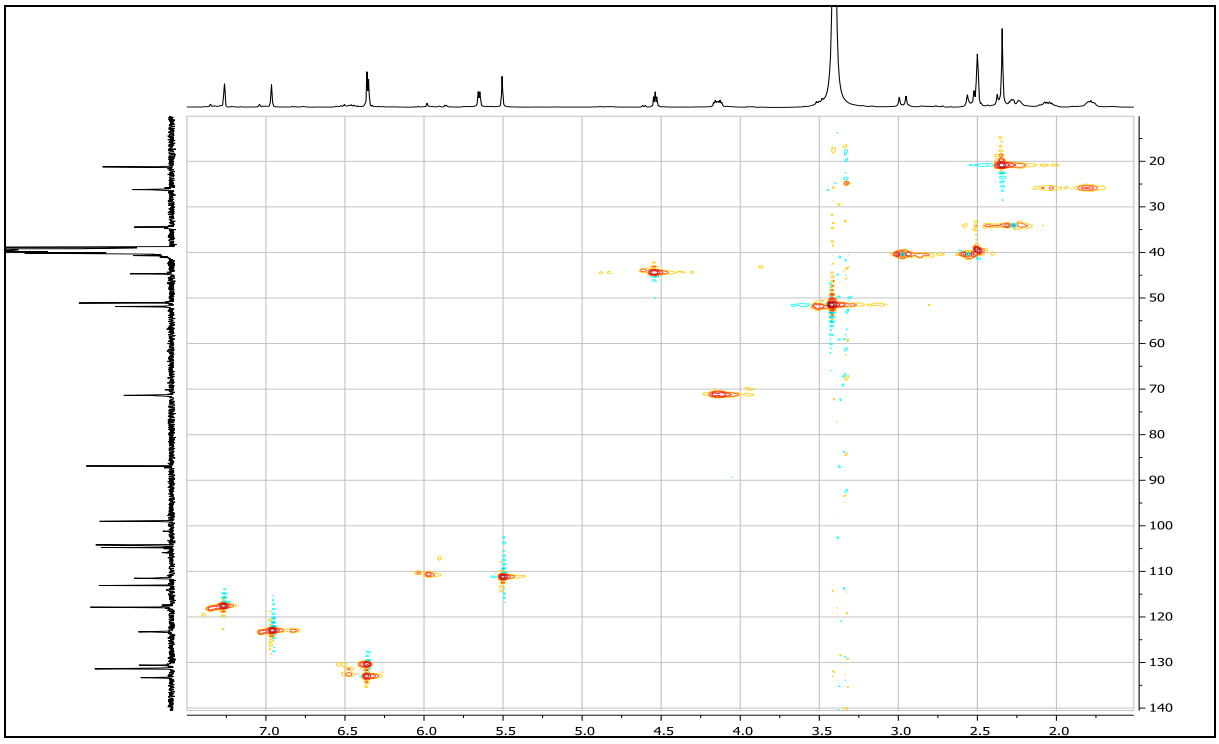

Figure S13. HSQC spectrum of compound **1** in DMSO-d_6.

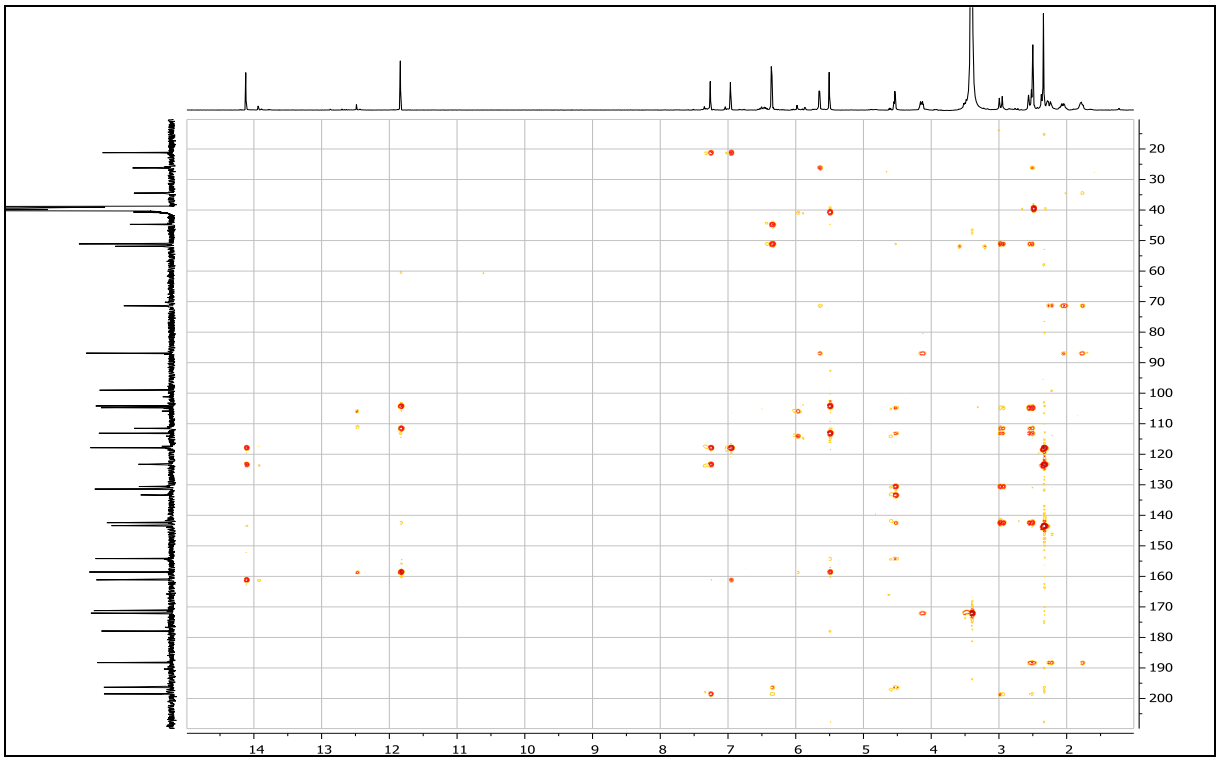

Figure S14. HMBC spectrum of compound **1** in DMSO-d_6.

Table S1. ^{1}H and ^{13}C NMR data of **1** (CD_3OD, 500 MHz) and xanthoquinodin B1 ($CDCl_3$, 400 MHz).

Position	**1**			Xanthoquinodin B1[a]	
	δ_H	δ_C	HMBC	δ_H	δ_C
2		87.6			84.6
3	4.22 (dd, 12.5, 4.5)	74.3	2, 4, 15	4.48 (dd, 4.0, 1.9)	66.9
4	2.20 (m)	26.0	2, 3, 5	2.18 (ddd, 14.5, 6.5, 4.0)	22.9
	1.98 (m)		2, 3, 5, 6	2.05 (m)	
5	2.69 (m)	36.0	4, 6	2.85 (ddd, 19.5, 12.0, 7.0)	24.4
	2.49 (dd, 18.0, 7.0)		3, 4, 6, 7	2.38 (dd, 19.5, 7.0)	
6		191.4			180.4
7		100.2			100.1
8		178.8			186.8
9		105.5			105.6
10		160.4			160.3
11	5.57 (s)	113.5	8, 9, 10, 13, 15'	6.17 (s)	113.9
12		144.8			146.5
13		114.2			114.2
14		155.4			153.8
15		174.9			170.9
16	3.59 (s)	52.9	15	3.76 (s)	53.5
1'		200.2			195.4
2'		133.4			132.2
3'	7.39 (s)	119.9	1', 5', 7', 16'	7.57 (d, 1.5)	121.0
4'		145.7			147.7
5'	6.98 (s)	124.6	3', 6', 7', 16'	7.09 (d, 1.0)	124.3
6'		162.8			164.4
7'		118.9			115.0
8'		176.4			183.2
9'		106.3			107.0
10'		199.2			188.4
11'	4.63 (d, 7.0)	46.0	12, 13, 14, 8', 9', 10', 12', 13'	4.79 (dd, 6.5, 1.0)	38.5
12'	6.34 (dd, 8.3, 7.0)	133.1	13, 9', 10', 11', 13', 14'	6.49 (dd, 8.0, 6.2)	131.2
13'	6.55 (d, 8.3)	133.4	13, 1', 9', 11', 12', 14'	6.69 (dd, 8.0, 1.0)	132.9
14'		53.3			49.9
15'	2.99 (d, 17.0)	41.8	10, 11, 12, 13, 14, 1', 9', 13', 14'	3.04 (d, 17.8)	38.8
	2.70 (d, 17.0)		10, 11, 12, 13, 14, 1', 9', 13', 14'	2.95 (d, 17.8)	
16'	2.38 (s)	21.7	3', 4', 5'	2.45 (s)	22.1
6-OH				14.10 (s)	
10-OH	12.12 (s)		9, 10, 11	11.27 (s)	
6'-OH	13.79 (brs)		5', 6', 7'	11.70 (s)	
8'-OH				14.98 (s)	

[a]Tabata, Tomoda, et al. 1993

Table S2. ^{1}H and ^{13}C NMR data of 1 (DMSO-d_6, 400 MHz).

	1		
Position	δ_H	δ_C	HMBC
2		87.3	
3	4.13 (td, 12.0, 4.4)	71.8	2, 15
4	2.03 (m)	26.6	2, 3, 5, 6
	1.76 (m)		
5	2.50 (m)	34.8	3, 6
	2.24 (m)		
6		188.7	
7		99.4	
8		178.3	
9		104.6	
10		159.0	
11	5.49 (s)	111.9	8, 9, 10, 13, 15'
12		142.8	
13		113.5	
14		154.6	
15		172.5	
16	3.39 (s)	52.3	15
1'		198.9	
2'		131.0	
3'	7.25 (s)	118.3	1', 5', 7', 16'
4'		143.8	
5'	6.94 (s)	123.7	3', 6', 7', 16'
6'		161.6	
7'		118.3	
8'		171.6	
9'		105.2	
10'		196.8	
11'	4.52 (dd, 4.4, 3.6)	45.1	13, 14, 9', 10', 12', 13'
12'	6.34 (brs)	133.7	10', 11', 14'
13'	6.35 (brs)	131.8	1', 11', 14'
14'		51.5	
15'	2.95 (d, 17.2)	41.1	11, 12, 13, 13', 14'
	2.52 (d, 17.2)		
16'	2.32 (s)	21.6	3', 4', 5'
3-OH	5.64 (s)		2, 4
10-OH	11.82 (s)		9, 10, 11
6'-OH	14.10 (s)		5', 6', 7'

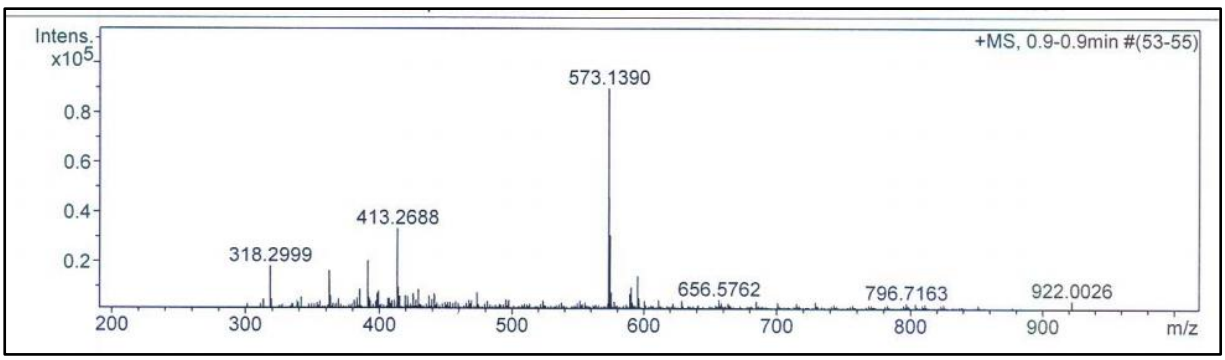

Figure S15. HRESITOFMS spectrum of compound **1.**

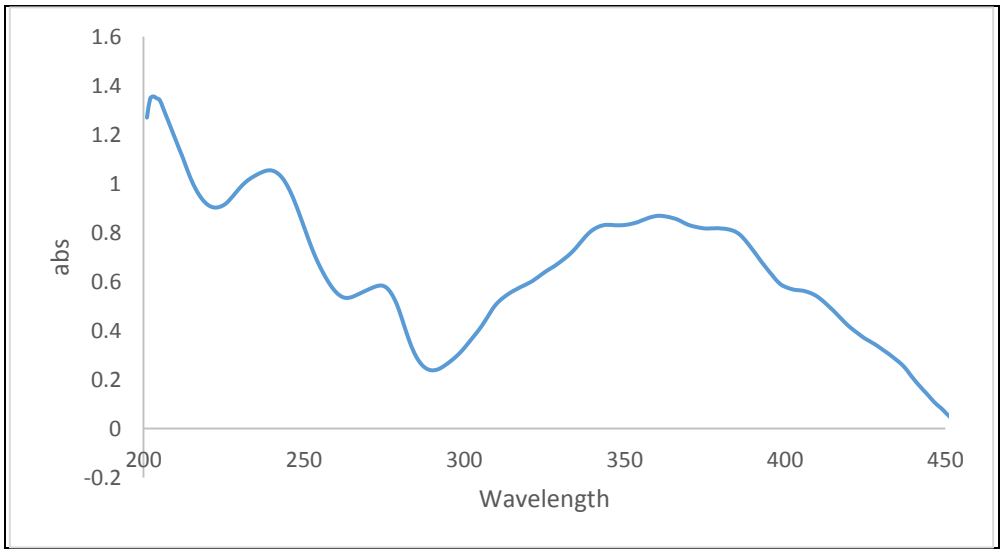

Figure S16. UV spectrum of compound **1**

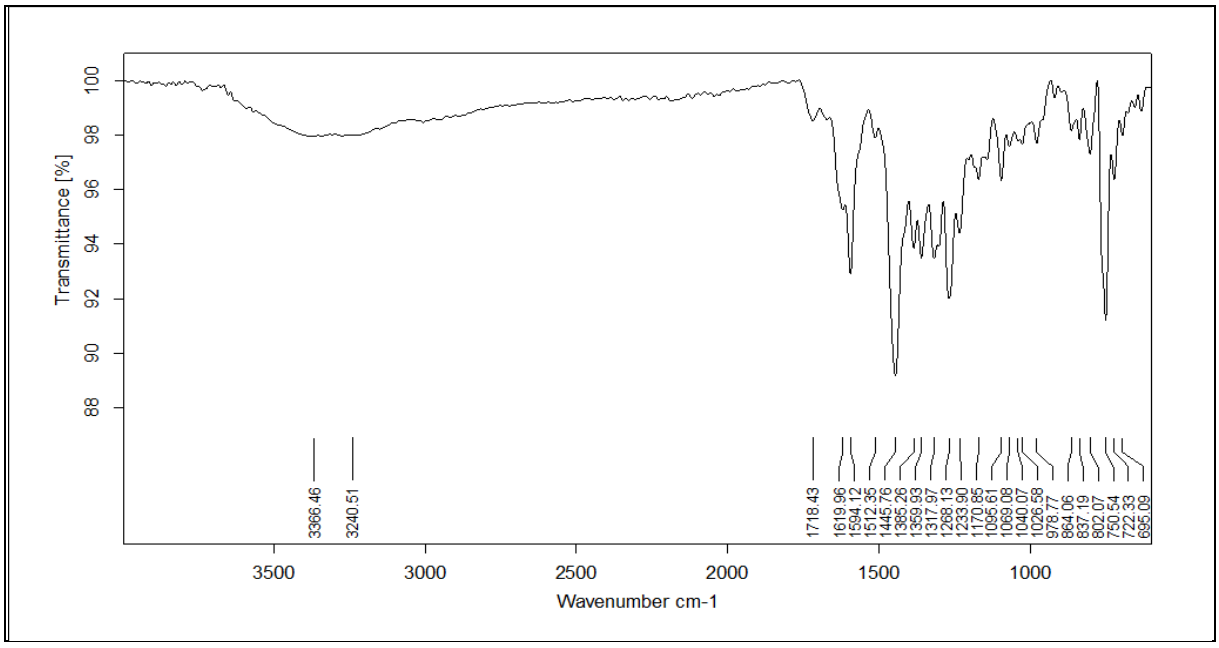

Figure S17. IR spectrum of compound **1**

Computational method of electronic circular dichroism (ECD) for 1

For theoretical ECD spectra, Conformation analysis of all structures were optimized by the B3LYP/6-31G(d,p) method and ECD spectra were calculated using the time dependent density functional theory (TD-DFT) method with CAM-B3LYP functional and 6-311++G (d,p) basis set. Conformers of **1d** and **1e** were selected with agreement with experimental ECD spectra and lowest energy. Polarizable Continuum Model (PCM) solvation model using methanol was included in the calculations. All calculations were performed using Gaussian09 program (Frisch et al. 2009), UV shifting (Bringmann et al. 2009) (−25 nm).

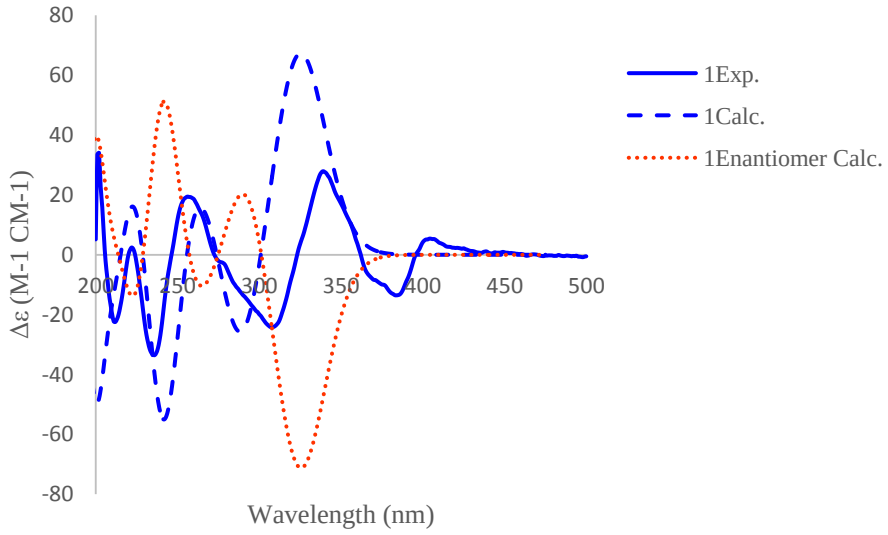

Figure S18. ECD spectra of xanthoquinodin B9 (**1**): Experimental ECD, calculated ECD (2*S*, 3*S*, 11'*S*, 14'*R*) and its calculated enantiomer ECD (2*R*, 3*R*, 11'*R*, 14'*S*) spectra.

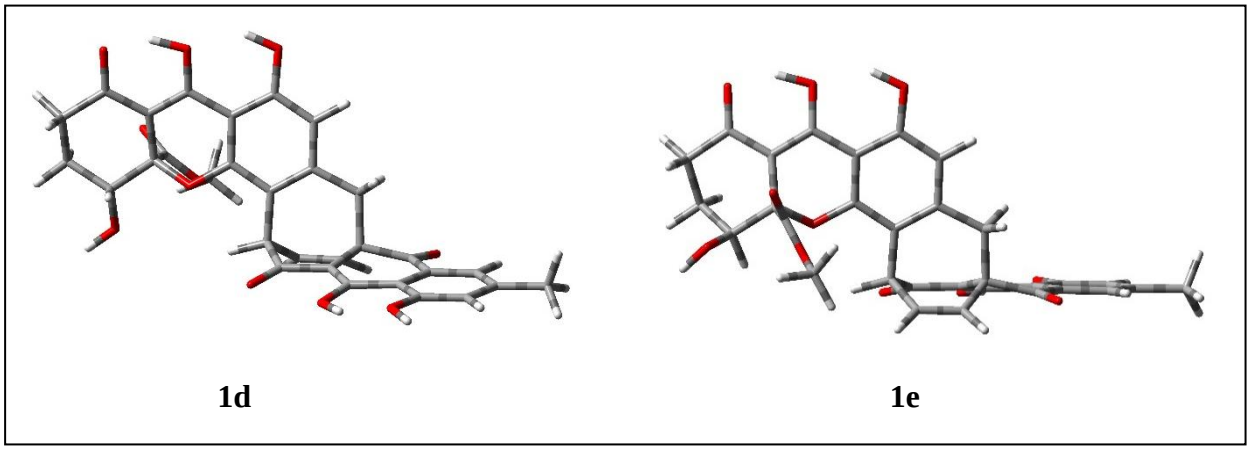

Figure S19. Optimized structures of all configuration using B3LYP/6-31G(d,p) level in methanol (PCM).

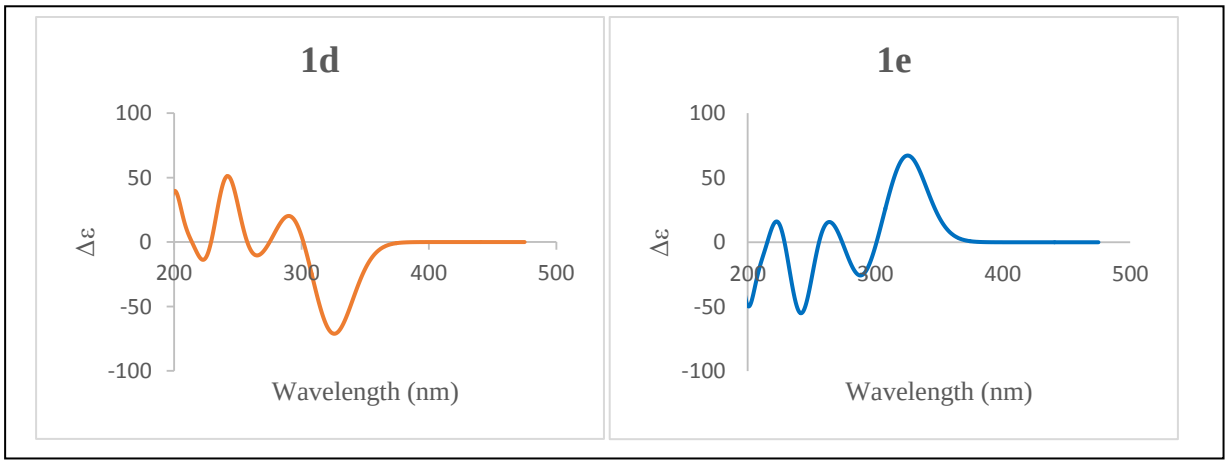

Figure S20. TDDFT calculated CD spectra of **1d** and **1e** at CAM-B3LYP/6-311++G(d,p) level in methanol (PCM).

Table S3**.** Calculated ECD spectra of configuration at TD-CAM-B3LYP/6-311++G(d,p) including PCM model (MeOH).

Compound	Calculated ECD			
	λ (nm)	*f*	R_{len}	Transition
d	353	0.3424	-70.27	148->150
	322	0.4110	11.10	147->151
	267	0.4189	51.21	145->150
	215	0.3014	-10.86	147->152
e	353	0.3344	66.07	148->150
	315	0.2699	-25.23	147->151
	267	0.4327	-55.02	145->150
	216	0.3165	14.13	149->155

λ = Wavelength
F = Oscillator strength.
R_{len} = Rotatory strength in length form

Configuration **1d**

HOMO

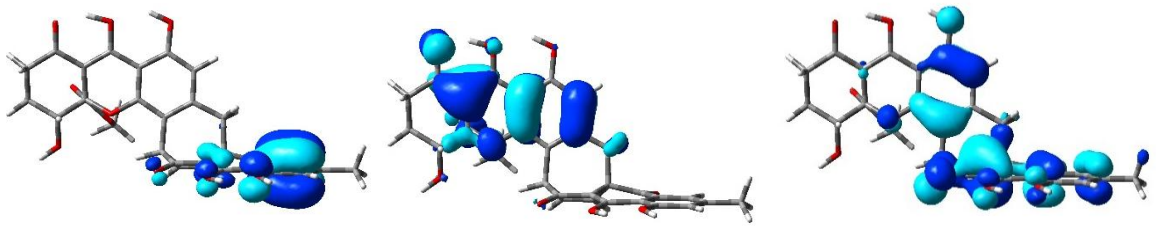

145 **147** **148**

LUMO

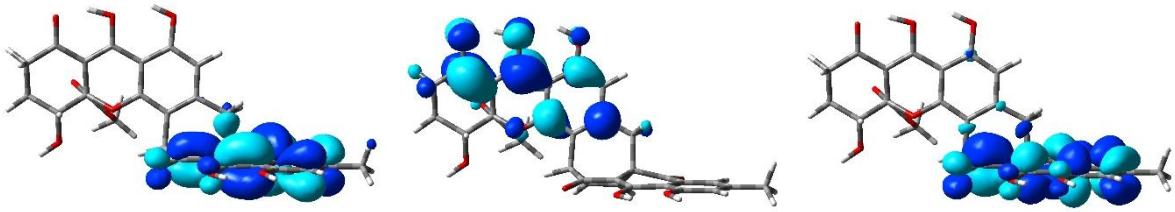

150 **151** **152**

Figure S21**.** Molecular orbitals of configuration **1d**.

Configuration **1e**

HOMO

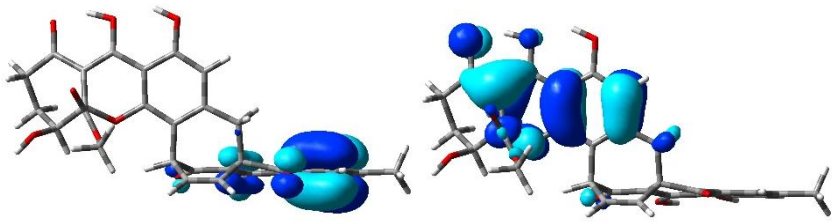

145 **147**

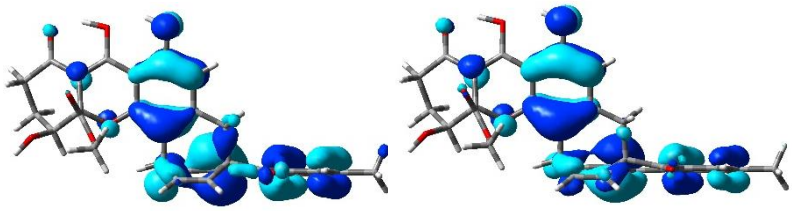

148 **149**

Figure S22**.** Molecular orbitals of configuration **1e**.

Biological assays

Antibacterial assay

Gram positive bacteria (*B. cereus* ATCC 11778, *S. aureus* ATCC 6538, and methicillin resistance *S. aureus* (MRSA)) and Gram negative bacteria (*Escherichia coli* ATCC 25922, *Pseudomonas aeruginosa* ATCC 27853, and *Salmonella typhimurium* ATCC 13311) were obtained from the Department of Microbiology, Faculty of Science, Khon Kaen University. Minimum inhibition concentration (MICs) were determined by a two-fold serial dilution method using Mueller Hinton broth (CLSI 2014). Briefly, serial 2-fold dilutions of samples in DMSO were mix with MHB in a 96-well microplate, 50 µl of bacteria was then added to each well (final concentration of 1×10^6 CFU/mL/well) and the plate was incubated at 35° for 16−18 hours. The MIC was determined after addition of resazurin (10 µl) for 2−3 hours and was observed colors (blue: active, pink: inactive). All samples were tested in triplicate and the standard drugs were vancomycin, kanamycin, and cefepime.

Antimalarial assay

Antimalarial activity was evaluated against the parasite *Plasmodium falciparum* (K1, multidrug resistant strain), using the method of Targer and Jensen (1976). Quantitative assessment of malarial activity in vitro was determined by means of a microculture radioisotope technique based upon the method of Desjardins (1979). The inhibitory concentration (IC_{50}) represents the concentration which causes 50% reduction in parasite growth as indicated by the in vitro uptake of [^{3}H]-hypoxanthine by *P. falciparum*. Dihydroartemisinine was used as a standard reference.

Antimycobacterial assay

Antimycobacterial activity was assessed against *Mycobacterium tuberculosis* H37Ra using the Microplate Alamar blue assay (MABA) (Collins and Franzblau 1997). Isoniazid was used as a reference compound.

Cytotoxicity assay

Cytotoxicity assays against human epidermoid carcinoma (KB), human breast adenocarcinoma (MCF7) and human small cell lung cancer (NCI-H187) were performed employing the colorimetric method as described by Skehan and coworkers (1990). The reference substances were doxorubicin and ellipticine.

Table S4. Antibacterial activity of compounds **1**−**6**.

Compound	Antibacterial activity (MIC, µM)					
	Gram positive bacteria			Gram negative bacteria		
	B. cereus	*S. aureus*	MRSA[a]	*E. coli*	*Ps. aeruginosa*	*Sa. typhimurium*
1	0.87	1.75	0.87	223.72	223.72	223.72
2	0.44	0.87	0.87	223.72	223.72	>223.72
3	0.22	1.75	1.75	223.72	223.72	>223.72
4	0.35	10.74[b]	0.02[b]	90.13	45.06	90.13
5	10.81	2.70	1.35	172.94	172.94	172.94
6	10.39	2.60	0.32	166.19	166.19	>166.19
vancomycin	1.35	0.67	0.67	-	-	-
kanamycin	3.43	1.72	-	6.87	-	-
cefepime	-	-	-	0.06	4.16	0.06

[a]methicillin resestance *S. aureus*
[b]picomolar (pM)

Table S5. Antimalarial, anti-TB activities, and cytotoxicity of compounds **1**−**6**.

Compound	Antimalarial (IC_{50}, μM)	Anti-TB[a] (MIC, μM)	Cytotoxicity (IC_{50}, μM)			
			KB[b]	MCF-7[c]	NCI-H187[d]	*Vero* cell[e]
1	2.57	87.39	7.04	18.40	0.98	1.78
2	2.55	87.39	6.54	8.60	1.03	2.90
3	6.29	Inactive	6.31	6.26	3.11	3.86
4	0.40	0.55	2.55	1.09	0.04	0.04
5	0.48	4.06	1.34	1.60	0.81	0.98
6	4.01	8.11	3.99	13.12	3.81	1.50
dihydroartemisinine	0.002	-	-	-	-	-
isoniazid	-	0.34	-	-	-	-
doxorubicin	-	-	1.07	17.24	0.40	-
ellipticine	-	-	8.97	-	9.54	4.22

[a]Anti-*Mycobacterium tuberculosis*
[b]Human epidermoid carcinoma in the mouth
[c]Human breast adenocarcinoma
[d]Human small cell lung cancer
[e]African green monkey kidney

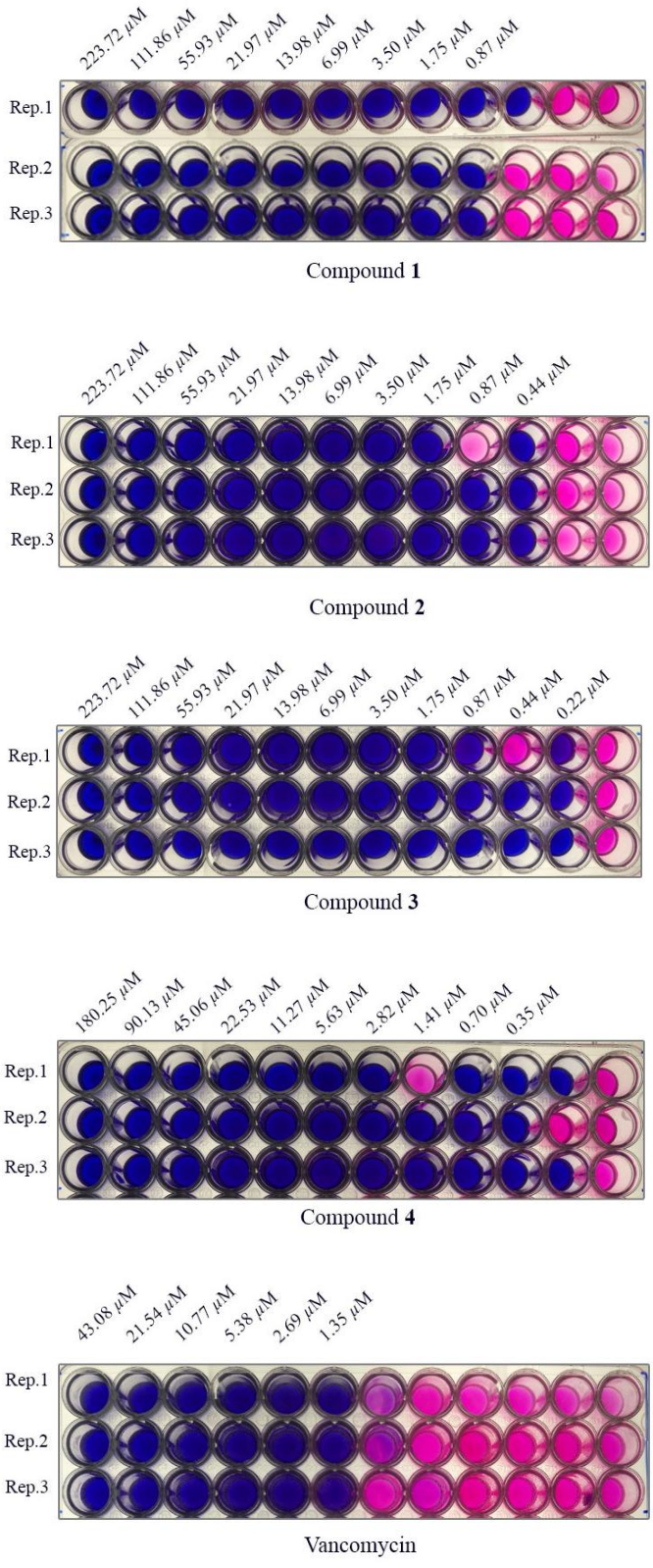

Figure S23. Antibacterial activity against *B. cereus* of compound **1**−**4** and vancomycin.

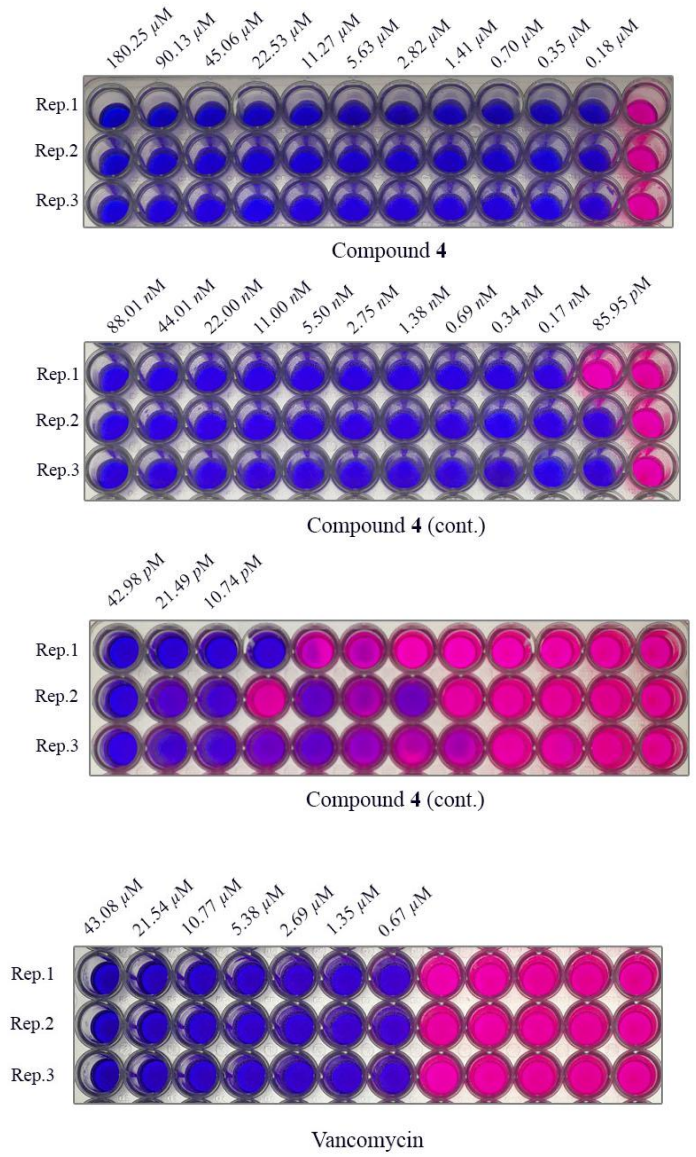

Figure S24. Antibacterial activity against *S. aureus* of compound **4** and vancomycin.

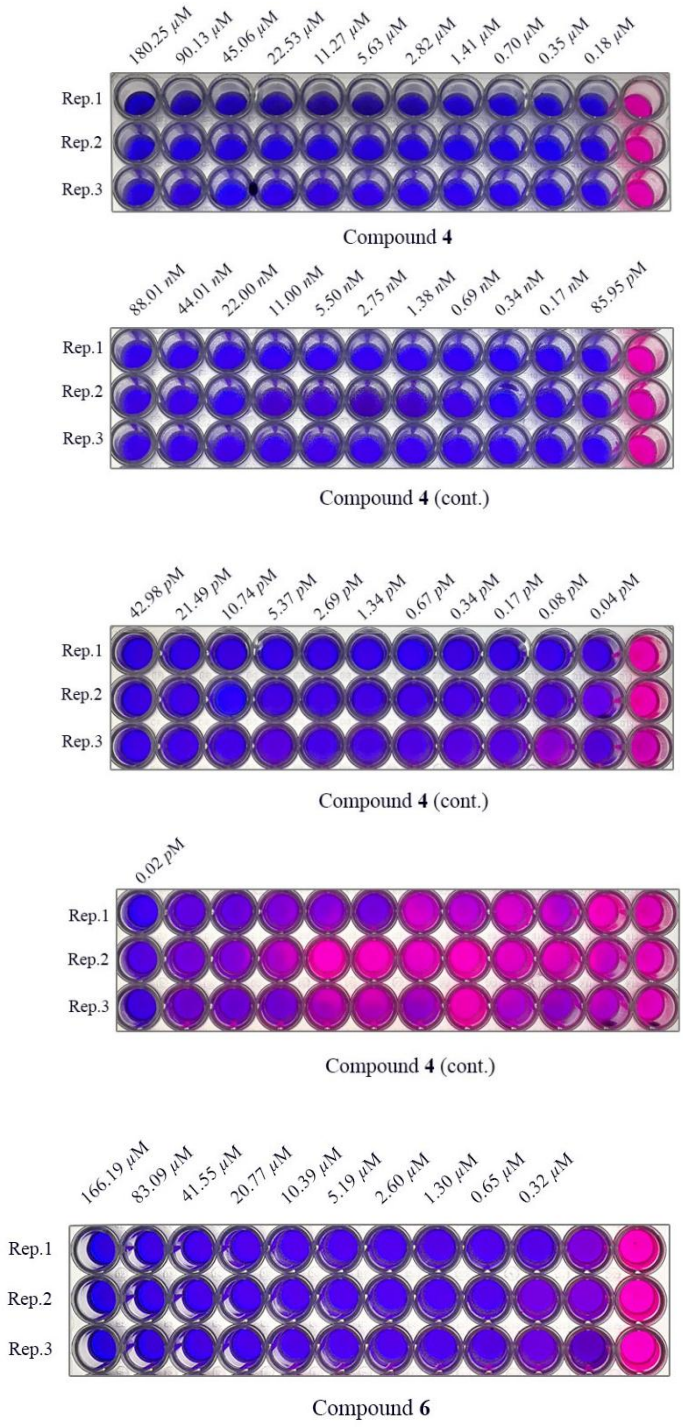

Figure S25. Antibacterial activity against MRSA of compounds **4** and **6**.

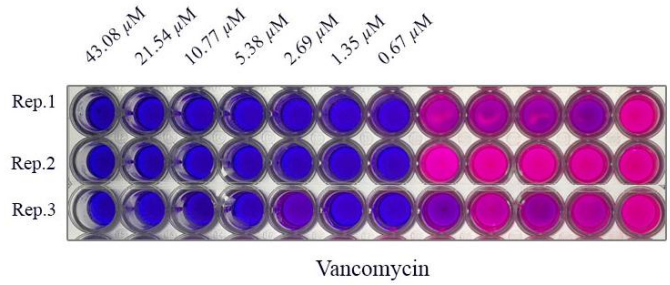

Figure S26. Antibacterial activity against MRSA of vancomycin.

References

Bringmann G, Bruhn T, Maksimenka K, Hemberger Y. 2009. The assignment of absolute stereostructures through quantum chemical circular dichroism calculations. Eur J Org Chem. 2009(17):2717−2727.

CLSI (Clinical and Laboratory Standards Institute). 2014. M100-S24 Performance standards for antimicrobial susceptibility testing; twenty-fourth informational supplement. Wayne, PA: Clinical and Laboratory Standards Institute.

Collins LA, Franzblau SG. 1997. Microplate Alamar blue assay versus BATEC 460 system for high-throughput screening of compounds against *Mycobacterium tuberculosis* and *Mycobacterium avium*. Antimicrob Agents Chemother. 41:1004−1009.

Desjardins RE, Canfield CJ, Haynes JD, Chulay JD. 1979. Quantitative assessment of antimalarial activity in vitro by a semiautomated microdilution technique. Antimicrob Agents Chemother. 16:710−718.

Frisch MJ, Trucks GW, Schlegel HB, Scuseria GE, Robb MA, Cheeseman JR, Scalmani G, Barone V, Mennucci B, Petersson GA, et al. 2009. Gaussian, Inc., Wallingford CT.

Skehan P, Storeng R, Scudiero D, Monks A, McMahon J, Vistica D, Warren JT, Bokesch H, Kenney S, Boyd MR. 1990. New colorimetric cytotoxicity assay for anticancer-drug screening. J Natl Cancer Inst. 82:1107−1112.

Tabata N, Tomoda H, Matsuzaki K, Omura S. 1993. Structure and biosynthesis of xanthoqunodins, anticoccidial antibiotics. 115:8558−8564.

Targer W, Jensen, JB. 1976. Human malaria parasites in continuous culture. Science. 193:673−675.